Springer

KSME

Journal of Mechanical Science and Technology 26 (4) (2012) 1089~1097
www.springerlink.com/content/1738-494x
DOI 10.1007/s12206-012-0225-x

Predictive carbon nanotube models using the eigenvector dimension reduction (EDR) method †

Zhimin Xi[1] and Byeng D. Youn[2,*]

[1]*Department of Industrial and Manufacturing Systems Engineering, University of Michigan – Dearborn, MI, 48168, USA*
[2]*School of Mechanical and Aerospace Engineering, Seoul National University, Seoul, Korea*

(Manuscript Received April 8, 2011; Revised September 13, 2011; Accepted December 29, 2011)

Abstract

It has been reported that a carbon nanotube (CNT) is one of the strongest materials with its high failure stress and strain. Moreover, the nanotube has many favorable features, such as high toughness, great flexibility, low density, and so on. This discovery has opened new opportunities in various engineering applications, for example, a nanocomposite material design. However, recent studies have found a substantial discrepancy between computational and experimental material property predictions, in part due to defects in the fabricated nanotubes. It is found that the nanotubes are highly defective in many different formations (e.g., vacancy, dislocation, chemical, and topological defects). Recent parametric studies with vacancy defects have found that the vacancy defects substantially affect mechanical properties of the nanotubes. Given random existence of the nanotube defects, the material properties of the nanotubes can be better understood through statistical modeling of the defects. This paper presents predictive CNT models, which enable to estimate mechanical properties of the CNTs and the nanocomposites under various sources of uncertainties. As the first step, the density and location of vacancy defects will be randomly modeled to predict mechanical properties. It has been reported that the eigenvector dimension reduction (EDR) method performs probability analysis efficiently and accurately. In this paper, molecular dynamics (MD) simulation with a modified Morse potential model is integrated with the EDR method to predict the mechanical properties of the CNTs. To demonstrate the feasibility of the predicted model, probabilistic behavior of mechanical properties (e.g., failure stress, failure strain, and toughness) is compared with the precedent experiment results.

Keywords: Carbon nanotube (CNT); Mechanical property; Vacancy defect; Uncertainty quantification; Eigenvector dimension reduction; Molecular dynamics

1. Introduction

Nanostructured materials have the potential to provide order-of-magnitude increases in stiffness-to-weight and strength-to-weight ratios relative to current materials used for structural engineering applications [1, 2] and for small-scale devices [3-5]. The material properties of the CNTs have been investigated thoroughly using molecular mechanics (MM), molecular dynamics (MD), and quantum mechanics (QM) methods [6-13]. The Young's moduli of the CNTs are around 1 TPa, which is comparable to the diamond. Table 1 summarizes both computational and experimental results for the material properties. Substantial difference is found between the computational and experimental results in prediction of the material properties. The difference is mainly due to the defects in the CNTs and the modeling/testing fidelity. Although QM simulation is considered to be the most accurate method, it is almost impossible to simulate the failure properties of the CNTs, due to its expensive computation. Given computational intensiveness, the MD simulations with empirical potential models, such as Brenner potential model, modified Morse potential model, and universal force model, are extensively used for material modeling. Most MD simulations have been focused on predicting material properties of defect-free nanotubes. As shown in Table 1, the recent studies reported that the defect-free CNTs have around 100 GPa of the failure stresses and 15-30% of the failure strain.

Compared with simulations, only small amount of experiments [14-16] have been carried out to measure the mechanical properties of the CNTs due to the small scale. As shown in Table 1, experimental approach has reported substantially lower values of failure stress and strain, for example, 11-63 GPa of the failure stress, 2-12% of the failure strain, and 270-950 GPa of Young's modulus for the CNTs [16].

One of the reasons for such discrepancy between simulations and experiments can be found in manufacturing defects

*Corresponding author. Tel.: +82 2 880 1919, Fax.: +82 2 880 8302
E-mail address: bdyoun@snu.ac.kr
† Recommended by Editor Maenghyo Cho

Table 1. Comparison of simulation and experiment results.

		Young's modulus (TPa)	Failure stress (GPa)	Failure strain (%)
Simulation	Yakobson et al. (1997) Theoretical study	1.067	300	30
	Lu (1997) Empirical force constant model	0.971 ~ 0.975	-	-
	Yao & Lordi (1998) Universal force field model	~1	-	-
	Zhou et al. (2000) Electronic energy band theory	1.065	-	-
	Belytschko et al. (2002) Modified Morse model	1.16	93.5	15.7
	Ogata & Shibutani (2003) Tight binding theory	0.965~0.979	-	-
	Mielke et al. (2004) Brenner potential model	0.78~0.92	88~105	18.1~29.7
	Sammalkorpi et al. (2004) Brenner potential model	0.67~0.7	-	-
Experiment	Wong et al. (1997)	0.69 ~ 1.87	-	-
	Salvetat et al. (1999)	0.81	-	-
	Yu et al. (2000)	0.27~0.95	11~63	2~12

in the nanotubes. It has reported [17] that the CNTs are highly defective by studying the radial compressibility and intercalation with potassium and rubidium. Vacancy defects due to irradiation effects [18-20] have been investigated and could be the most important reason causing such a large discrepancy between simulations and experiments. The CNTs manufactured using injection chemical vapor decomposition (CVD) method have been reported full of defects [21]. Therefore, the defective CNTs should be considered in simulations to explain such a discrepancy.

A few simulations have been carried out [10, 12, 13] to study the influence of vacancy defects to the failure stress, failure strain, and Young's modulus of the CNTs. The trend is observed that more vacancy defects cause the inferior mechanical properties of the CNTs. Even if the number and types of defects and their locations are conceived to be random, no research has attempted to explain such discrepancy from the statistical point of view. For material design, it is critically important to predict mechanical properties of the CNTs with consideration of random manufacturing defects. The long-term objective of this research is to develop a multiscale predictive model for composite materials reinforced by the CNTs, as shown in Fig. 1. This research proposes a predictive model for the CNTs with consideration of random manufacturing defects. First, this study investigates the effect of radius and length effects on the material properties of the defect-free CNTs. Then, the number of vacancy defects is considered as random parameter. In the presence of the vacancy defects in the CNTs, the material properties are predicted statistically. The eigenvector dimension reduction (EDR) method is employed for predictive modeling of the CNTs.

Uncertainty quantification is of critical importance to understand random nature of physics in engineering systems.

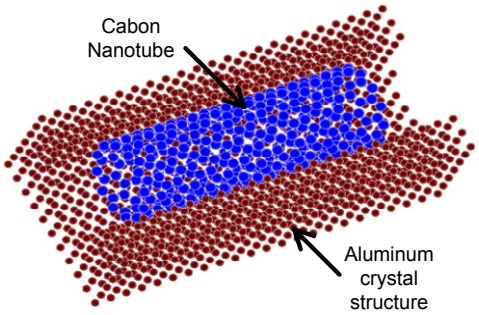

Fig. 1. Composite material reinforced by the CNTs.

However, a common challenge in uncertainty quantification is a multi-dimensional integration to quantify probabilistic nature of a system. It is almost impossible to conduct the multi-dimensional integration analytically and direct numerical integration is not feasible due to its computational cost. Other than direct numerical or analytical integration methods, existing methods for uncertainty quantification can be categorized into four groups: 1) sampling method; 2) expansion method; 3) the most probable point (MPP)-based method; and 4) approximate integration method.

The sampling method is the most comprehensive but considerably expensive to use for estimating statistical moments of system responses. So, it is often used for verification of uncertainty quantification analysis when alternative methods are employed. The idea of the expansion method is to estimate statistical moments of system responses with a small perturbation to simulate input uncertainty. This expansion method includes Taylor expansion, perturbation method [22, 23], the Neumann expansion method [24], etc. All expansion methods could become computationally inefficient or inaccurate when

the number or the degree of input uncertainty is higher. Moreover, since it requires high-order partial sensitivities of system responses, it is not practical for the applications of the CNTs. The MPP-based method has widely been used to perform reliability analysis. Rotationally invariant reliability index is introduced through a nonhomogeneous transformation [25]. However, the MPP-based method requires the first-order sensitivities of system responses. So, it is not applicable for the discrete variable of vacancy defects in the CNTs.

The approximate integration method is a direct approach to estimate the PDF (or statistical moments) through numerical integration. This paper integrates the eigenvector dimension-reduction (EDR) method [26] for the uncertainty quantification of mechanical properties of the CNTs. It has been shown that the EDR method is the most accurate and efficient method for the uncertainty quantification. In this paper, a brief review of EDR method is firstly presented. Next, mechanical properties of the CNTs (failure stress, failure strain and toughness) with respect to vacancy defects are carried out at the EDR eigenvector sample points. Finally, Probability density functions (PDFs) of mechanical properties are constructed based on the assumed input vacancy uncertainty.

2. Review of eigenvector dimension reduction (EDR) method

In general, statistical moments (or PDF) of system responses can be calculated as

$$\mathbf{E}\left\{Y^m(\mathbf{X})\right\} = \int_{-\infty}^{+\infty}\cdots\int_{-\infty}^{+\infty} Y^m(\mathbf{x})\cdot f_{\mathbf{V}}(\mathbf{x})\cdot d\mathbf{x} \tag{1}$$

in Eq. (1), a major challenge is a multi-dimensional integration over the entire random input domain. To resolve this difficulty, the EDR method uses an additive decomposition [27] that converts a multi-dimensional integration in Eq. (1) into multiple one-dimensional integrations. Thus, Eq. (1) can be approximated as

$$\mathbf{E}\left[Y^m(\mathbf{X})\right] \cong \mathbf{E}\left[\overline{Y}^m(\mathbf{X})\right] = \int_{-\infty}^{\infty}\cdots\int_{-\infty}^{\infty} \overline{Y}^m\cdot f_{\mathbf{X}}(\mathbf{x})\cdot d\mathbf{x} \tag{2}$$

where

$$\overline{Y} = \sum_{j=1}^{N} Y(\mu_1,...,\mu_{j-1},X_j,\mu_{j+1},...,\mu_N) - (N-1)\cdot Y(\mu_1,...,\mu_N)\,.$$

Using a binomial formula, Eq. (2) can be evaluated by executing one-dimensional integration recursively. Uncertainty of system responses can be evaluated through multiple one-dimensional numerical integrations. The challenge of the problem still remains how to carry out one dimensional integration effectively.

To overcome the challenge, the EDR method incorporates three technical components: (1) eigenvector sampling, (2) one-dimensional response approximations for efficient and accurate numerical integration, and (3) a stabilized Pearson system for PDF generation.

2.1 Eigenvector sampling

Accuracy for probability analysis can be increased as the number of integration points becomes larger in recursive one-dimensional integration. However, the increase of integration points makes simulations prohibitively expensive. To achieve both accuracy and efficiency in probability analysis, one dimensional response surface will be created using samples along the eigenvectors of a random system. For efficiency, the EDR method employs only either three or five samples along each eigenvector, depending on nonlinearity of the system responses. For N number of random variables, the EDR method demands $2N$+1 or $4N$+1 samples including the design point.

To obtain the eigenvectors and eigenvalues, an eigen-problem can be formulated as

$$\mathbf{\Sigma X} = \lambda\mathbf{X} \tag{3}$$

where $\mathbf{X}$ and λ are eigenvectors and eigenvalues of the covariance matrix, $\mathbf{\Sigma}$. Depending on statistical configuration of the system, four different types of problems can be defined: (a) uncorrelated and symmetric, (b) correlated and symmetric, (c) uncorrelated and asymmetric, and (d) correlated and asymmetric. For any circumstance, eigenvector samples will be found at

$${}^1X_i' = \mu_i - k\sqrt{\lambda_i} \text{ and } {}^2X_i' = \mu_i + k\sqrt{\lambda_i} \tag{4}$$

where X_i' and λ_i are the i^{th} eigenvector and eigenvalue, and k determines samples along the eigenvectors. The eigenvector samples are used for constructing one-dimensional response approximation using SMLS method in the following section.

2.2 Stepwise moving least squares (SMLS) method for numerical integration

The moving least squares (MLS) method [28] is improved by a stepwise selection of basis functions, referred to as the stepwise moving least squares (SMLS) method. The optimal set of basis terms is adaptively chosen to maximize numerical accuracy by screening the importance of basis terms. This technique is exploited for approximating the integrand in Eq. (2). The idea of a stepwise selection of basis functions comes from the stepwise regression method [29]. The SMLS method allows the increase in the number of numerical integration points without requiring actual system evaluations through simulations or experiments. Thus, a large number of integration points can be used to increase numerical accuracy in assessing statistical moments of the responses while maintaining high efficiency. The EDR method has no restriction to choose numerical integration schemes.

2.3 A stabilized Pearson system

The Pearson system [30] can be used to construct the PDF

of a random response (Y) based on its first four moments (mean, standard deviation, skewness and kurtosis). The detail expression of the PDF can be achieved by solving the differential equation as

$$\frac{1}{p(Y)}\frac{dp(Y)}{dY} = -\frac{a+Y}{c_0 + c_1 Y + c_2 Y^2} \tag{5}$$

where a, c_0, c_1 and c_2 are four coefficients determined by the first four moments of the random response (Y) and expressed as

$$c_0 = (4\beta_2 - 3\beta_1)(10\beta_2 - 12\beta_1 - 18)^{-1}\mu_2$$
$$a = c_1 = \sqrt{\beta_1}(\beta_2 + 3)(10\beta_2 - 12\beta_1 - 18)^{-1}\sqrt{\mu_2}$$
$$c_2 = (2\beta_2 - 3\beta_1 - 6)(10\beta_2 - 12\beta_1 - 18)^{-1}$$

where β_1 is the square of skewness, β_2 is the kurtosis, and μ_2 is the variation. The mean value is always treated as zero in the Pearson System, and it can be easily shifted to the true mean value once the differential equation is solved. Basically, the differential equation can be solved based on the different assumptions of the four coefficients a, c_0, c_1, and c_2. For example, if c_1=c_2=0, this equation can be solved with a normal distribution, and the type 1 in Pearson system corresponds to both roots of c_0+c_1Y+c_2Y^2 being real. In Pearson system, however, a singularity problem is often found due to the fail of calculating coefficients of a specific distribution type, which results in a numerical instability.

In the EDR method, a stabilized Pearson system is proposed to avoid instability. Two hyper-PDFs are generated by fixing the first three statistical moments, and incrementally adjusting the original kurtosis by slightly increasing or decreasing the value until two hyper-PDFs are successfully constructed. Then these two hyper-PDFs are used to approximate the PDF with original moments.

3. Computational methods

In an MD simulation, some popular potential models are available such as Tersoff-Brenner models [31-33], a modified Morse model [10], and a universal force field (UFF) model [34]. Different models could produce different mechanical properties of the CNTs. It is found using three different models that the size effect [35] on the Young's modulus of the CNTs is insignificant when a tube diameter is larger than 2 nm. However, when the tube diameter is less than 2nm, all three different models show significant discrepancy in the predicted Young's moduli. In this paper, modified Morse potential model is employed because its result is close to those from the QM simulation, compared to the other models [10].

3.1 Modified Morse potential and force model

The potential energy of atom i can be expressed as

$$E_i = E_{stretch} + E_{angle} \tag{6}$$

where $E_{stretch}$ and E_{angle} are the potential energies for two-atom and three-atom interactions, respectively, and expressed as

$$E_{stretch} = D_e\left\{\left[1 - e^{-\beta(r_{ij\_d} - r_0)}\right]^2 - 1\right\} \tag{7}$$

$$E_{angle} = \frac{1}{2}k_\theta(\theta_{ijk} - \theta_0)^2\left[1 + k_{sextile}(\theta_{ijk} - \theta_0)^4\right] \tag{8}$$

where

$r_0 = 1.39(\mathring{A}), D_e = 3.7647(eV), \beta = 2.625(1/\mathring{A}), \theta_0 = 2.094(rad),$
$k_\theta = 5.618(eV/rad^2), k_{sextile} = 0.754(rad^{-4})$

and r_{ij_d} is the distance between two atoms, and θ_{ijk} is the bond angle among three atoms.

In the MD simulations, the force acting on each atom must be calculated to simulate the motion of atom. Basically, the force acting on each atom i is the first derivative of its potential energy with respect to the position and can be obtained as

$$F_i = -\frac{\partial E_i}{\partial r_i} = -\left(\frac{\partial E_{stretch}}{\partial r_i} + \frac{\partial E_{angle}}{\partial r_i}\right). \tag{9}$$

The detail derivation of the atomic forces is given in Appendix A.1.

3.2 Formulation of uncertainty of vacancy defects

Since the number of missing atoms (or defects) must be a non-negative random variable, a bounded distribution must be used with a lower bound a = 0. Although the number of defects is discrete, a continuous distribution will be considered because a defect density (continuous random variable) will be employed in future research. The number of vacancy defects is assumed to be a 4-parameter Beta distribution defined as

$$p(x) = \frac{(x-a)^{p-1}(b-x)^{q-1}}{B(p,q)(b-a)^{p+q-1}} \qquad a \le x \le b; \quad p,q > 0 \tag{10}$$

where p and q are the shape parameters, a and b are the lower and upper bounds, respectively, of the density function, and $B(p,q)$ is the beta function. The upper bound (b) is assumed to be 10. The mean and standard deviation of beta distribution is assumed to be 5 and 1, respectively. The density function of vacancy defects is shown in Fig. 2. Then, the eigenvector samples for the number of vacancy defects using the EDR method are 2, 5, and 8. Using the MD simulation, the mechanical properties of the CNTs at the eigenvector samples are computed to further construct the density function of mechanical properties. In this paper, vacancy defects are assumed to be concentrated in the CNTs, as shown in Fig. 3.

It has been reported [19] that vacancy defects can be mended through atomic rearrangements, referred to as surface

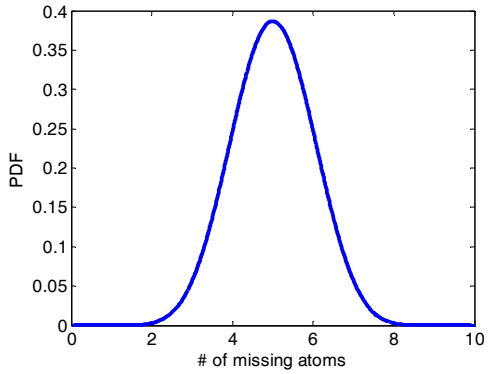

Fig. 2. Distribution of number of missing atoms.

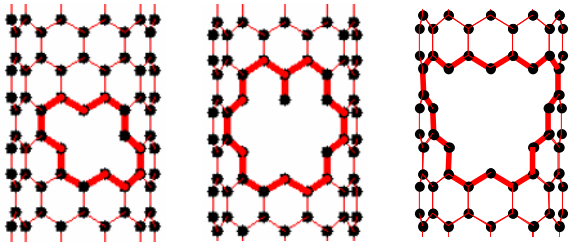

(a) 2 atom vacancy (b) 5 atom vacancy (c) 8 atom vacancy

Fig. 3. Vacancy defects of carbon nanotube.

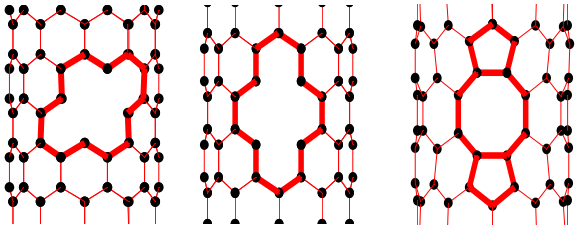

(a) (b) (c)

Fig. 4. Two-atom vacancy and surface reconstruction.

reconstruction. It has also been observed [36] that surface reconstruction is unnecessary if an initial configuration of vacancy defects is sufficiently stable. Therefore, in this paper, the stability of vacancy defects is firstly studied using the modified Morse potential model. It is found that for the same number of vacancy defects, the CNT surface could remain same in Fig. 4(a) or reconstructed from Fig. 4(b) to Fig. 4(c). For example, in a 2-atom vacancy defect case, there are two possible constructions as shown in Fig. 4(a) and (b). The former is very stable, so the reconstruction is unnecessary. But the later is unstable so that atoms are easily rearranged to form a more stable configuration, as shown in Fig. 4(c). It must be aware that for the same number of vacancy defect, the mechanical properties, such as failure stress and failure strain, could be slightly different whether or not a surface reconstruction is considered. In this paper, however, only relatively stable structures without surface reconstruction are considered, since this paper is focused on a predictive model development

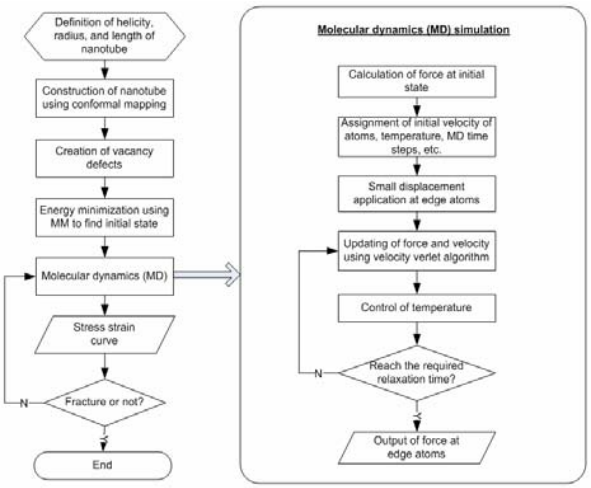

Fig. 5. Flowchart of the MD simulation process.

with consideration of random vacancy defects.

3.3 MD simulation process

For a given configuration of the CNTs, a conformal mapping method [37] is employed to construct the CNTs. Then, any vacancy defects corresponding to the eigenvector sample points are implemented in the CNTs. In order to find the initial state of the CNTs, the molecular mechanics (MM) simulation is employed to minimize the potential energy of the CNTs. Then the CNTs are stretched with a small displacement at one end of the CNTs and keep the other end fixed. After the stretch, force relaxation must be done with a small strain rate. The forces and stresses at the stretched end of the CNTs are recorded during this tensile simulation test until the CNTs are fractured. For any displacement increment, the MD simulation employs a velocity verlet algorithm to update the velocity and location of atoms with the time step of 0.5 fentosecond. At the same time, a velocity rescaling method is used to control the temperature of simulation system at 300 K. The flowchart of the MD simulation is shown in Fig. 5.

4. Results and discussion

In this paper, the [10,0] CNT with the length of 6nm is mainly used to study probabilistic behavior of mechanical properties of the CNTs. In this study, smaller diameter of the CNTs is used, compared with the CNTs, [150,0] to [450,0], used in the experiment. It is mainly because of a computational expense. Based on the previous reported results [12] using Tersoff-Brenner potential model, no difference is found in both failure stress and strain for the CNTs with small and large diameters. Considering the length, there is around 1% difference of failure strain for short and long nanotube, and the failure stress is almost the same for both cases. Although the simulation results for the [10,0] CNT is comparable to those from the experiment, a special caution must be paid because

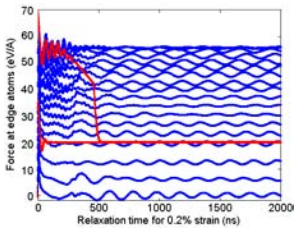

(a) Force relaxation with 0.1%/ps strain rate

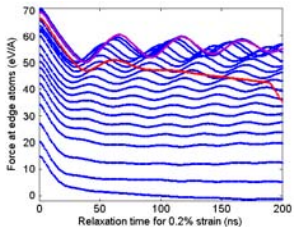

(b) Force relaxation with 1%/ps strain rate

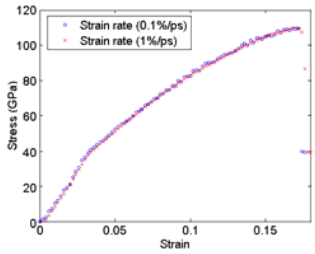

(c) Stress-strain curves of 1%/ps and 0.1%/ps strain rate

Fig. 6. Study of strain rate effect.

the modified Morse model is employed in this paper and inconsistence to Young's moduli using these two models has been observed [35]. Therefore, the effect on the mechanical properties is investigated with the modified Morse potential model and the [10,0] CNTs. Strain rate is another important factor that could cause artificially higher failure stress and strain in the MD simulation [38].

4.1 Strain rate effect

It has been observed [38] that a substantial difference of the strain rate between the MD simulations and experiments could be one of the reasons causing a high failure strain in the simulations. Due to the time scale (fentosecond) used in the MD simulations, the strain rate in the MD simulations is usually on the order of 0.1%~1%/picosecond, however, in the experiments, a strain rate as 0.1%~1%/minute is usually applied. Thus, a slow enough strain rate must be identified to avoid artificially high failure strain or failure stress. In this example, the [10,0] defect-free CNT with around 2nm of length is tested with 0.1%/ps and 1%/ps strain rate. In both cases, 0.2% strain (0.004nm displacement) is applied at one end of the CNT at each stretching process. For 0.1%/ps and 1%/ps strain rate, 2000 ns and 200 ns are used for the relaxation of 0.2% strain. The forces applied at the edge atoms with reduced unit (eV/A) are recorded for the whole tensile test process. In order to make it easy to identify the shape of force curve during the relaxation time, the curves are displayed for every 1% strain applied to the nanotube. It can be observed from Fig. 6(a) and Fig. 6(b) that the forces acting on the edge atoms are first sharply decreased because of the sudden displacement applied at the edge atoms, then gradually converged to stable values

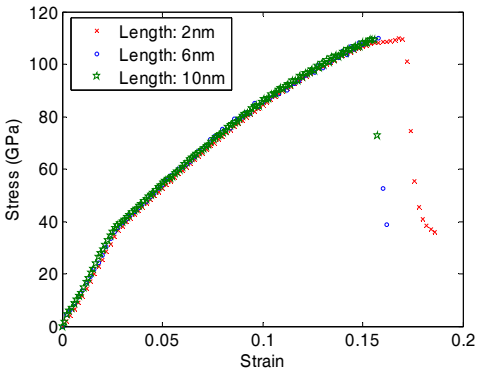

Fig. 7. Study of length effect.

with sufficient time for the force relaxation. The average force is obtained in the last 100 ns at all strain values. The curves are shown in blue color if no fracture failure of the nanotube is observed; otherwise red color is used to denote the fracture failure, which is indicated by the drop of the average force during the tensile simulation. The force relaxation is performed with a slow relaxation rate (0.1%/ps) in Fig. 6(a) and with a fast strain rate (1%/ps) in Fig. 6(b). In both cases, the corresponding stress-strain curves are displayed in Fig. 6(c). The curves with two different strain rates are almost identical. Therefore, the faster strain rate can be used to save computational time. However, the failure stress and strain can be overestimated with more than 1%/ps of strain rate. For the longer CNTs, a longer relaxation time is necessary to make the forces converge to a stable state. Thus, it is important to identify a proper strain rate to achieve an accurate and efficient estimate of mechanical properties.

4.2 Length effect

The length of the CNTs is directly related with the computation time of the MD simulation. It has been found [12] that a long nanotube always produces smaller failure strain compared with a short one (~ 2 nm) although the difference seems to be small (around 1%). However, failure stresses remain constant for the short and long nanotubes. In this paper, the length effect is studied with the modified Morse potential to find the minimal length of the CNTs required for the predictive CNT model. This study employs the [10,0] CNTs with the lengths of 2 nm, 6 nm, and 10nm. The stress strain curves for those CNTs are shown in Fig. 7. The consistent result to the previous study [12] is obtained, which gives smaller failure strain and slightly higher stress throughout the stress-strain curve for the longer CNT. The differences of failure strain and stress between 2 nm and 6 nm CNTs are 1.4% and 0.3 GPa, respectively. However, the difference between 6 nm and 10 nm CNTs is found to be negligible. Therefore, this study suggests to use 6 nm CNT considering computational efficiency and accuracy.

Table 2. Mechanical properties of the CNTs.

# of Vacancy Defect	0	2	5	8
Failure Strain (%)	15.8	10.8	8.2	6.4
Failure Stress (GPa)	110.1	84.9	64.3	50.2
Toughness (GPa)	11.6	6.1	3.5	2.1

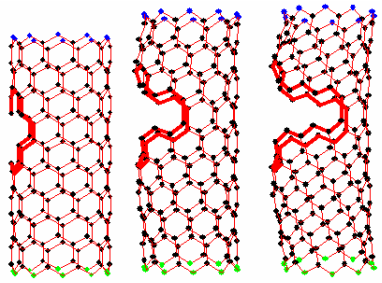

Fig. 8. Fracture process of the CNT with five defects.

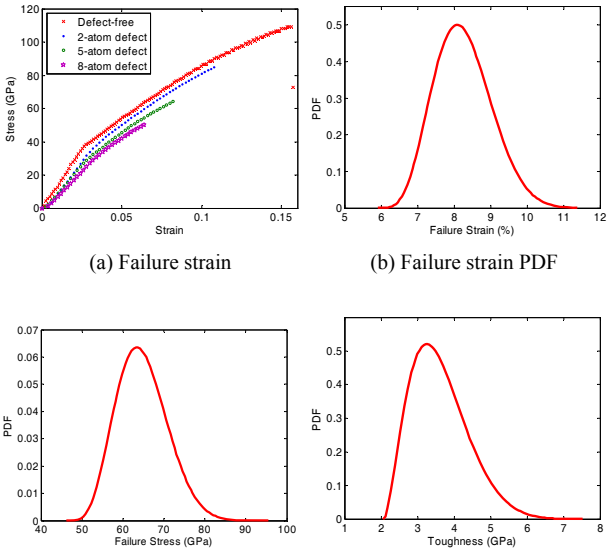

(a) Failure strain (b) Failure strain PDF

(c) Failure stress PDF (d) Toughness PDF

Fig. 9. Stress-strain curves and PDF of mechanical properties.

4.3 Uncertainty quantification of mechanical properties

At the eigenvector sample points (2, 5, and 8 atom defects), the MD simulations are carried out using the [10,0] carbon nanotube with the length of 6nm. For the CNT with five vacancy defects, a fracture process is displayed in Fig. 8. The mechanical properties are listed in Table 2 for both defect-free and defective CNTs. The stress-strain curves are shown in Fig. 9(a). It is found that vacancy defects significantly reduce the failure stress, failure strain and toughness. The Young's modulus is also slightly reduced by vacancy defects. Using the information at the eigenvector sample points, the EDR method is employed to construct the probability density function of mechanical properties with consideration of random vacancy defects (the mean $\mu = 5$ and the standard deviation $\sigma = 1$ for the number of vacancy defects). The results are shown in Fig. 9(b)-(d) for [10,0] carbon nanotube with a solid line. It is observed that failure strain is in the range of 6%-11%, which is consistent with experiment results. However, failure stresses are mostly located from 50-90 GPa, which are slightly higher than the experiment results 11-63 GPa.

5. Conclusion

This paper presents a predictive CNT model that enables to study the probabilistic nature for mechanical properties of the CNTs using the EDR method. It is found that vacancy defects can significantly affect the mechanical properties of the CNTs. Furthermore, under the assumption on the random property of vacancy defects, the EDR method produces the PDF of mechanical properties with three simulations. Although the predicted failure strain is close to the experiment result, the predicted failure stress is still higher compared with the experiment result. Based on the findings in this paper, the following research topics will be further investigated in near future. First, the size effect study with different radii will be carried out, which will provide a good comparative result between simulation and experiment. Next, a defect density in the CNTs will be considered as a random parameter. Finally, the mechanical properties of nanocomposites reinforced by the CNTs will be predicted in multi-length scales under various sources of manufacturing uncertainties.

Acknowledgements

Research was supported by the SNU-IAMD (Seoul National University-Institute of Advanced Machinery and Design), the National Research Foundation of Korea (NRF) grant funded by the Korea government (No. 2011-0022051), and the Faculty Research Initiation and Seed Grant at University of Michigan – Dearborn.

Nomenclature

$f_X(x)$: Probability density function of random variables X
$Y(x)$: System response of input random variables X
E : Expectation operator
N : Total number of input random variables
$\bar{Y}$: Approximated system response
$\boldsymbol{\Sigma}$: Covariance matrix
λ : Eigenvalues
$E_{stretch}$: Potential energies for two-atom interactions
E_{angle} : Potential energies for three-atom interactions
r_{ij_d} : Distance between two atoms
θ_{ijk} : Bond angle among three atoms
F_i : Force acted on i^{th} atom

References

[1] R. H. Baughman, A. A. Zakhidov and W. A. D. Heer, Carbon nanotubes-the route toward applications, *Science,* 297

(2002) 787-792.
[2] D. Srivastava, C. Wei and K. Cho, Nanomechanics of carbon nanotubes and composites, *Applied Mechanics Reviews*, 56 (2003) 215-230.
[3] P. Ajayan and T. Ebbesen, Nanometre-size tubes of carbon, *Reports on Progress in Physics*, 60 (1997) 1025-1062.
[4] C. Dekker, Carbon nanotubes as molecular quantum wires, *Physics Today*, 52 (1999) 22-28.
[5] P. Harris, *Carbon nanotubes and related structures: new materials for the 21st century*, Cambridge University Press (1999).
[6] J. P. Lu, Elastic properties of carbon nanotubes and nanoropes, *Physical Review Letters*, 79 (1997) 1297-1300.
[7] B. I. Yakobson, M. P. Campbell, C. J. Brabec and J. Bernholc, High strain rate fracture and C-chain unraveling in carbon nanotubes, *Computafional Materials Science*, 8 (1997) 341-348.
[8] N. Yao and V. Lordi, Young's modulus of single-walled carbon nanotubes, *Journal of Applied Physics*, 84 (1998) 1939-1943.
[9] Z. Xin, Z. Jianjun, Ou-Yang and Zhong-can, Strain energy and Young's modulus of single-wall carbon nanotubes calculated from electronic energy-band theory, *Physical Review B*, 62 (2000) 13692-13696.
[10] T. Belytschko, S. P. Xiao, G. C. Schatz and R. S. Ruoff, Atomistic simulations of nanotube fracture, *Physical Review B,* 65 (2002) 235430-235438.
[11] S. Ogata and Y. Shibutani, Ideal tensile strength and band gap of single-walled carbon nanotubes, *Physical Review B*, 68 (2003) 165409-165412.
[12] S. Mielke, D. Troya, S. Zhang, J. Li, S. Xiao and R. Car, The role of vacancy defects and holes in the fracture of carbon nanotubes, *Chemical Physics Letters,* 390 (2004) 413-420.
[13] M. Sammalkorpi, A. Krasheninnikov and A. Kuronen, Mechanical properties of carbon nanotubes with vacancies and related defects, *Physical Review B*, 70 (2004) 245416-245423.
[14] E. W. Wong, P. E. Sheehan and C. M. Lieber, Nanobeam mechanics: elasticity, strength, and toughness of nanorods and nanotubes, *Science*, 277 (1997) 1971-1975.
[15] J. P. Salvetat, G. A. D. Briggs, J. M. Bonard, R. R. Bacsa, A. J. Kulik, T. Stöckli, N. A. Burnham and L. Forró, Elastic and shear moduli of single-walled carbon nanotube ropes, *Physical Review Letters*, 82 (1999) 944-947.
[16] M. F. Yu, O. Lourie, M. J. Dyer, K. Moloni, T. F. Kelly, and R. S. Ruoff, Strength and breaking mechanism of multiwalled carbon nanotubes under tensile load, *Science*, 287 (2000) 637-640.
[17] O. Zhou, R. M. Fleming, D. W. Murphy, C. H. Chen, R. C. Haddon, A. P. Ramirez and S. H. Glarum, Defects in carbon nanostructures, *Science*, 263 (1994) 1744-1747.
[18] B. Smith and D. Luzzi, The physics of electronic and atomic collisions, NY, *AIP Conf. Proc.* (1995).
[19] P. M. Ajayan, V. Ravikumar and J. C. Charlier, Surface reconstructions and dimensional changes in single-walled carbon nanotubes, *Physical Review Letters,* 81 (1998) 1437-1440.
[20] F. Banhart, Irradiation effects in carbon nanostructures, *Reports on Progress in Physics,* 62 (1999) 1181-1221.
[21] Z. E. Horvátha, K. Kertésza, L. Pethőa, A. A. Koósa, L. Tapasztóa, Z. Vértesya, Z. Osvátha, A. Darabontb, P. Nemes-Inczeb, Z. Sárközib and L. P. Biróa, Inexpensive, upscalable nanotube growth methods, *Current Applied Physics*, 6 (2006) 135-140.
[22] M. Kleiber and H. T. D, *The stochastic finite element method*, New York, Wiley (1992).
[23] S. Rahman and B. N. Rao, A perturbation method for stochastic meshless analysis in elastostatics, *International Journal for Numerical Methods in Engineering*, 50 (2001) 1961-1991.
[24] F. Yamazaki and M. Shinozuka, Neumann expansion for stochastic finite element analysis, *Journal of Engineering Mechanics*, 114 (1988) 1335-1354.
[25] A. M. Hasofer and N. C. Lind, Exact and invariant second-moment code for-mat, *Journal of the Engineering Mechanics*, 100 (1974) 111-121.
[26] B. D. Youn, Z. Xi and P. Wang, Eigenvector dimension-reduction (EDR) method for sensitivity-free uncertainty quantification, *Structural and Multidisciplinary Optimization*, 37 (2008) 13-28.
[27] S. Rahman and H. Xu, A univariate dimension-reduction method for multi-dimensional integration in stochastic mechanics, *Probabilistic Engineering Mechanics*, 19 (2004) 393-408.
[28] B. D. Youn and K. K. Choi, A new response surface methodology for reliability-based design optimization, *Computers and Structures*, 82 (2004) 241-256.
[29] H. R. Myers and D. C. Montgomery, Response surface methodology, New York, Wiley (1995).
[30] N. Johnson, S. Kotz and N. Balakrishnan, *Continuous univariate distributions*, New York, Wiley (1995).
[31] J. Tersoff, New empirical approach for the structure and energy of covalent systems, *Physical Review B*, 37 (1988) 6991-7000.
[32] D. W. Brenner, Empirical potential for hydrocarbons for use in simulating the chemical vapor deposition of diamond films, *Physical Review B*, 42 (1990) 9458-9471.
[33] D. W. Brenner, O. A. Shenderova, J. A. Harrison, S. J. Stuart, B. Ni and S. B. Sinnott, A second-generation reactive empirical bond order (REBO) potential energy expression for hydrocarbons, *Journal of Physics: Condensed Matter*, 14 (2002) 783-802.
[34] A. K. Rappé, C. J. Casewit, K. S. Colwell, W. A. Goddard III and W. M. Skiff, UFF, a full periodic-table force-field for molecular mechanics and molecular dynamics simulations, *J. Amer. Chem. Soc.* 114 (1992) 10024-10035.
[35] S. P. Xiao and W. Y. Hou, Studies of size effects on carbon nanotubes' mechanical properties by using different potential functions, *Fullerenes, Nanotubes, and Carbon Nanostruc-*

tures, 14 (2006) 9-16.

[36] A. V. Krasheninnikov, K. Nordlund, M. Sirvio, E. Salonen, and J. Keinonen, Formation of ion-irradiation-induced atomic-scale defects on walls of carbon nanotubes, *Physical Review B*, 63 (2001) 245405-245410.

[37] C. T. White, D. H. Robertson and J. W. Mintmire, Helical and rotational symmetries of nanoscale graphitic tubules, *Physical Review B*, 47 (1993) 5485-5488.

[38] C. Wei, K. Cho and D. Srivastava, Tensile strength of carbon nanotubes under realistic temperature and strain rate, *Physical Review B*, 67 (2003) 115407-115412.

Appendix

A.1. Derivation of atomic force

$$\frac{\partial E_{stretch}}{\partial r_i} = 2\beta D_e e^{-\beta(r-r_0)}\left(1-e^{-\beta(r-r_0)}\right)\frac{\partial r_{ij\_d}}{\partial r_i} \tag{A1}$$

$$\begin{aligned}\frac{\partial E_{angle}}{\partial r_i} &= \frac{\partial E_{angle}}{\partial \theta_{ijk}}\frac{\partial \theta_{ijk}}{\partial \cos\theta_{ijk}}\frac{\partial \cos\theta_{ijk}}{\partial r_i} \\ &= -k_\theta\left(\theta_{ijk}-\theta_0\right)\left[1+3k_{sextile}\left(\theta_{ijk}-\theta_0\right)^4\right]\frac{1}{\sin\theta_{ijk}}\frac{\partial \cos\theta_{ijk}}{\partial r_i}\end{aligned} \tag{A2}$$

where

$$\frac{\partial r_{ij\_d}}{\partial r_i} = -\frac{\vec{r}_{ij}}{r_{ij\_d}};\ \ and\ \vec{r}_{ij} = (x_j - x_i)\hat{x} + (y_j - y_i)\hat{y} + (z_j - z_i)\hat{z}.$$

The bond angle among atoms i, j, and k is defined as:

$$\cos\theta_{ijk} = \frac{\vec{r}_{ij}\cdot\vec{r}_{ik}}{r_{ij\_d}r_{ik\_d}} = \frac{x_{ij}x_{ik}+y_{ij}y_{ik}+z_{ij}z_{ik}}{\sqrt{x_{ij}^2+y_{ij}^2+z_{ij}^2}\sqrt{x_{ik}^2+y_{ik}^2+z_{ik}^2}}. \tag{A3}$$

The derivative of $\cos\theta_{ijk}$ with respect to the position of atom i can be expressed as:

$$\frac{\partial \cos\theta_{ijk}}{\partial r_i} = \frac{\partial \cos\theta_{ijk}}{\partial x_i}\hat{x} + \frac{\partial \cos\theta_{ijk}}{\partial y_i}\hat{y} + \frac{\partial \cos\theta_{ijk}}{\partial z_i}\hat{z} \tag{A4}$$

where

$$\begin{cases}\dfrac{\partial \cos\theta_{ijk}}{\partial x_i} = \dfrac{\partial \cos\theta_{ijk}}{\partial x_{ij}}\dfrac{\partial x_{ij}}{\partial x_i} + \dfrac{\partial \cos\theta_{ijk}}{\partial x_{ik}}\dfrac{\partial x_{ik}}{\partial x_i} = -\left(\dfrac{\partial \cos\theta_{ijk}}{\partial x_{ij}} + \dfrac{\partial \cos\theta_{ijk}}{\partial x_{ik}}\right) \\ \dfrac{\partial \cos\theta_{ijk}}{\partial y_i} = \dfrac{\partial \cos\theta_{ijk}}{\partial y_{ij}}\dfrac{\partial y_{ij}}{\partial y_i} + \dfrac{\partial \cos\theta_{ijk}}{\partial y_{ik}}\dfrac{\partial y_{ik}}{\partial y_i} = -\left(\dfrac{\partial \cos\theta_{ijk}}{\partial y_{ij}} + \dfrac{\partial \cos\theta_{ijk}}{\partial y_{ik}}\right) \\ \dfrac{\partial \cos\theta_{ijk}}{\partial z_i} = \dfrac{\partial \cos\theta_{ijk}}{\partial z_{ij}}\dfrac{\partial z_{ij}}{\partial z_i} + \dfrac{\partial \cos\theta_{ijk}}{\partial z_{ik}}\dfrac{\partial z_{ik}}{\partial z_i} = -\left(\dfrac{\partial \cos\theta_{ijk}}{\partial z_{ij}} + \dfrac{\partial \cos\theta_{ijk}}{\partial z_{ik}}\right).\end{cases}$$

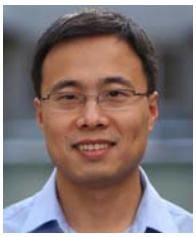

Zhimin Xi is a Research Assistant Professor in the Department of Industrial and Manufacturing Systems Engineering at the University of Michigan – Dearborn. He received his B.S. and M.S. degree in mechanical engineering from Beijing University of Science and Technology and his Ph.D from University of Maryland - College Park. He is the one-time winner of the Best Paper Award from ASME International Design Engineering Technical Conference (IDETC) in 2008. His research interests are robust/reliability based design, multi-scale materials and product design, and model validation & verification.

Byeng D. Youn is an Assistant Professor in the School of Mechanical and Aerospace Engineering at Seoul National University, South Korea. He received his B.S. degree in mechanical engineering from Inha University, his M.S. degree in mechanical engineering from KAIST, Korea and his Ph.D from the University of Iowa, USA. He is the two-time winner of the Best Paper Award from ASME International Design Engineering Technical Conference (IDETC) in 2001 and 2008. His research interests include computer model verification and validation, prognostics and health management, reliability analysis and reliability-based design, and energy harvester design.